JOURNAL OF THERMOPHYSICS AND HEAT TRANSFER
Vol. 28, No. 4, October–December 2014

Thermal Spreading Resistance Inside Anisotropic Plates with Arbitrarily Located Hotspots

A. Gholami* and M. Bahrami†
Simon Fraser University, Surrey, British Columbia V3T 0A3, Canada

DOI: 10.2514/1.T4428

Graphite-based anisotropic materials are becoming the key component of next-generation cooling systems in electronics and telecommunication industries. Proper use of these materials in the form of thermal spreaders, compared to conventional metallic ones, can significantly reduce the thermal stress and thermal resistance in the system. In this study, a new analytical model for temperature distribution inside anisotropic rectangular plates subjected to multiple sources and sinks on the top and bottom surfaces is presented. All lateral faces are assumed insulated. The solution is first justified for the case with single hotspots on each side and then using the superposition principle, it is extended into the general form to cover multihotspot cases. The model is validated by numerical simulation data and a perfect agreement is observed. Thermal spreading resistance is defined for the anisotropic plate and a comprehensive parametric study for optimization purpose is performed. The influence of both anisotropy and geometrical parameters on the resistance is discussed in detail and critical values are evaluated.

Nomenclature

A, B, C	=	solution coefficients
a	=	length of source/sink, m
b	=	width of source/sink, m
H	=	plate thickness, m
k	=	thermal conductivity, $\mathrm{W/m \cdot K}$
L	=	plate length, m
M	=	number of sources/sinks on top surface
m, n	=	term number in series solution
N	=	number of sources/sinks on bottom surface
Q	=	total heat flow, W
q	=	heat flux, $\mathrm{W/m^2}$
Q_{ref}	=	reference heat flow, W
s	=	Fourier series coefficient
T	=	temperature, K
T_0	=	reference temperature, K
W	=	plate width, m
X	=	x coordinate of source/sink center, m
Y	=	y coordinate of source/sink center, m
β	=	eigenvalue, z direction
δ	=	eigenvalue, y direction
ε	=	width to length aspect ratio of plate
ε_H	=	height to length aspect ratio of plate
κ	=	dimensionless thermal conductivity
λ	=	eigenvalue, x direction

Subscripts

i	=	number of sources/sinks on each surface
source	=	pertaining to heat sources
sink	=	pertaining to heat sinks

Superscripts

b	=	bottom surface
t	=	top surface
*	=	specifies dimensionless parameter
‘	=	pertaining to bottom surface

Received 7 March 2014; revision received 8 May 2014; accepted for publication 9 May 2014; published online 22 August 2014.

*M.Sc. Student, Laboratory for Alternative Energy Conversion, School of Mechatronic Systems Engineering, 8888 University Dr., Burnaby, BC V5A 1S6.

†Associate Professor, Laboratory for Alternative Energy Conversion, School of Mechatronic Systems Engineering, 8888 University Dr., Burnaby, BC V5A 1S6.

I. Introduction

RECENTLY, graphite-based anisotropic materials have received significant attention due to their exceptional thermophysical properties [1–3]. Graphite-based materials are one of the well-known anisotropic materials that have in-plane thermal conductivities, up to 1500 $\mathrm{W/m \cdot K}$, and through-plane thermal conductivities around 2 $\mathrm{W/m \cdot K}$ [3–6]. This property is mainly due to their special atomic structure. Generally, they are a stack of graphene flakes piled upon each other (Fig. 1). The interlayer cohesive energy of graphene flakes, which is due to the van der Waals atomic attraction, is much stronger than intralayer covalent bonding [7]. This structural feature causes large anisotropy in graphite, which makes it an ideal candidate for heat spreaders where higher heat transfer is desired in in-plane than in the through-plane direction. Heat spreaders are one of the main components in any cooling systems of electronic, power electronic, photonics, and telecom devices. They reduce heat flux at hotspots by spreading it into a larger area [8,9]. The spreading (or constriction) resistance causes an extra resistance against the heat flow, which can be minimized by properly designing the spreader.

A number of relevant analytical and numerical studies can be found on this topic in the literature. Most of the existing works were focused only on isotropic materials. Kokkas [10] obtained a general quasi-equilibrium Fourier–Laplace transform solution for a rectangular slab with heat sources on top and convective cooling on the bottom. Kadambi and Abuaf [11] developed an analytical solution to axisymmetric as well as three-dimensional (3-D) steady-state and transient heat conduction equations for a convectively cooled slab with a heat source at the center of the top surface. A numerical technique was presented by Albers [12] to solve for surface temperature of a stack of rectangular layers for both isotropic and anisotropic materials. Yovanovich et al. [8] reported a general expression for spreading resistance of a heat source centered on a rectangular double layer plate with either conduction or convection on the bottom surface. They also presented closed-form spreading resistance relationships for several special cases. Culham et al. [13] reported a more general solution to the 3-D Laplace equation for the rectangular plate with a centered heat source on the top and edge cooling instead of insulation on the sidewalls. Later, Muzychka et al. [14] extended the work of Culham et al. and solved the same problem in cylindrical coordinates for a circular slab. In another study, Muzychka et al. [15] reported a general solution for thermal spreading resistances of a convectively cooled rectangular flux

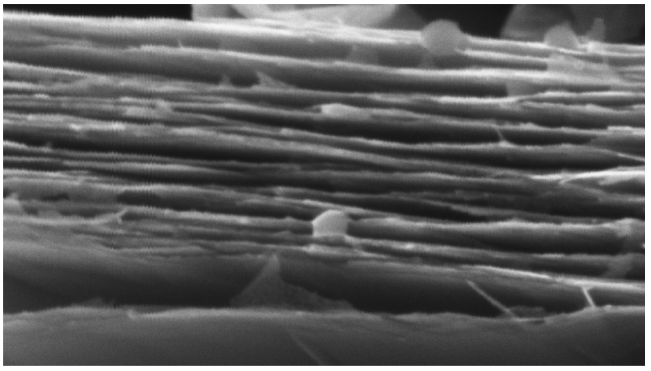

Fig. 1 SEM image of compressed expanded graphite.

channel with eccentric heat sources on top. Using a superposition technique, Muzychka [16] generalized the solution for problems with multiheat sources on the top. He introduced the "influence coefficient," which defines the contribution of each heat source on the temperature rise of other hotspots. Employing an asymptotic approach, Karmalkar et al. [9] proposed a closed-form expression for the spreading resistance for all rectangular and circular hotspot contact conditions. Rahmani and Shokouhmand [17,18] also investigated the effect of the temperature dependency of thermal conductivity on spreading resistance in semiconductors and, using the Kirchhoff transformation technique, they introduced spreading resistance models for different materials. Recently, Dan et al. [19] presented a solution to temperature distribution inside a multilayered isotropic rectangular tube with discrete isothermal hotspots on both top and bottom surfaces. To overcome the complexity of the mixed boundary conditions, they employed an approximate technique to convert this boundary condition into a Neumann boundary condition.

There are only a few analytic studies in the literature on 3-D conduction heat transfer in anisotropic materials subjected to discrete heat flux. Ying and Toh [20] developed an anisotropic spreading resistance model in cylindrical coordinates for a disc with a centric heat source on the top and convective cooling on the bottom. Muzychka et al. [21] brought a summary of all the previous studies for isotropic materials and, by transforming the boundary conditions and governing equations for anisotropic systems, obtained a new solution for convectively cooled rectangular flux channels as well as circular flux tubes with centralized heat source on the top. Muzychka recently proposed a thermal spreading resistance model for compound orthotropic systems with interfacial resistance subjected to a centric source on the top and convective cooling on the bottom for both rectangular and circular geometries [22,23].

In the present study, a new general solution to 3-D conduction heat transfer in an anisotropic rectangular plate ($k_x \neq k_y \neq k_z$) with multiple heat sources and heat sinks on the top and bottom surfaces is presented. The present model is validated by an independent numerical study. It is found that in electronic devices where heat is required to travel in-plane from the hotspot to get to the sink, which is the case of notebooks and cell phones, properly designed anisotropic spreaders perform much better than conventional isotropic metallic ones.

II. Model Development

An anisotropic rectangular plate of $L \times W$ with thickness of H (Fig. 2a) is considered for the following two scenarios:

1) Subjected to a single rectangular heat source and heat sink arbitrarily located on both the top and bottom surfaces. Heat source and sink refer to any type of heat inflow and outflow, respectively, whose profile of heat flux is known.

2) More generally, subjected to M and N, arbitrarily located sinks and sources on the top and bottom surface.

As boundary conditions, it is assumed that the lateral faces of the plate are insulated, i.e., there is no heat transfer through the sidewalls. All the top and bottom surfaces, except at the spots (refers to either source or sink), are also considered to be insulated. Spots have arbitrary heat flux, $q_{i(x,y)}$ (i is the number assigned to spots), positive values for heat sources, and negative values for sinks, which are functions of x and y. Each spot is centrally positioned at the x coordinate of X and y coordinate of Y, with a length and width of a and b, respectively, as shown in Fig. 2b. The objectives are to: 1) find the temperature distribution inside the plate with any arbitrary arrangement of spots on the top and bottom surfaces analytically and 2) define corresponding spreading resistance.

A. General Solution

Dimensionless parameters are defined as follows and the governing equation and boundary conditions are expressed accordingly

$$\varepsilon = \frac{W}{L}, \quad \varepsilon_H = \frac{H}{L}, \quad x^* = \frac{x}{L}, \quad y^* = \frac{y}{W}, \quad z^* = \frac{z}{H}$$
$$a_i^* = \frac{a_i}{L}, \quad b_i^* = \frac{b_i}{W}, \quad q_{i(x,y)}^* = \frac{LWq_{i(x,y)}}{Q_0}, \quad \theta = \frac{Lk_0}{Q_0}(T - T_0)$$
$$\kappa_x = \sqrt{\frac{k_0}{k_x}}, \quad \kappa_y = \sqrt{\frac{k_0}{k_y}}, \quad \kappa_z = \sqrt{\frac{k_0}{k_z}}, \quad R^* = Lk_zR \tag{1}$$

where Q_0 and k_0 are arbitrary reference heat flux and thermal conductivity, respectively, and T_0 is a reference temperature. Using the parameters in Eq. (1), the dimensionless form of the governing equation and the boundary conditions are

$$\nabla^2\theta = \frac{1}{\kappa_x^2}\frac{\partial^2\theta}{\partial x^{*2}} + \frac{1}{\varepsilon^2\kappa_y^2}\frac{\partial^2\theta}{\partial y^{*2}} + \frac{1}{\varepsilon_H^2\kappa_z^2}\frac{\partial^2\theta}{\partial z^{*2}} = 0 \tag{2}$$

$$\frac{\partial\theta}{\partial x^*} = 0 \text{ at } x^* = 0, \qquad x^* = 1$$
$$\frac{\partial\theta}{\partial y^*} = 0 \text{ at } y^* = 0, \qquad y^* = 1 \tag{3}$$

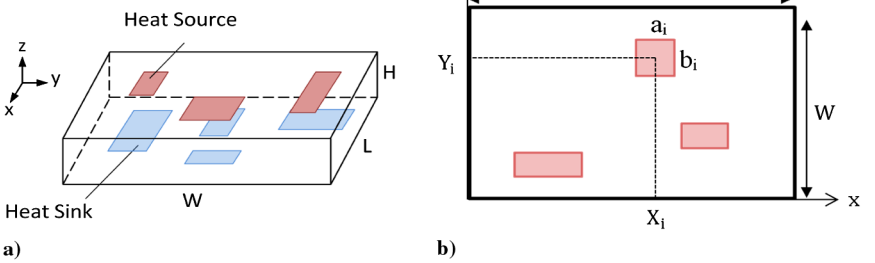

a) b)

Fig. 2 Schematic of anisotropic rectangular spreader with multiple hotspots on a) top and bottom surfaces size and b) location of hotspots.

$$\text{at } z^*=0 \rightarrow \begin{cases} \dfrac{\partial\theta}{\partial z^*}=\dfrac{\kappa_z^2\varepsilon_H}{\varepsilon}q^*_{i(x,y)} & \text{at spot } i \text{ domain} \\ \dfrac{\partial\theta}{\partial z^*}=0 & \text{at remainder} \end{cases}$$

$$\text{at } z^*=1 \rightarrow \begin{cases} \dfrac{\partial\theta}{\partial z^*}=\dfrac{\kappa_z^2\varepsilon_H}{\varepsilon}q'^*_{i(x,y)} & \text{at spot} i \text{ domain} \\ \dfrac{\partial\theta}{\partial z^*}=0 & \text{at remainder} \end{cases} \tag{4}$$

Using a separation of variable technique, Eq. (2) has the general solution in the form given next

$$\theta=\sum_{\lambda}\sum_{\delta}C_{(\lambda,\delta)}e^{\lambda\kappa_x x^*}e^{\delta\varepsilon\kappa_y y^*}e^{i\sqrt{\lambda^2+\delta^2}\varepsilon_H\kappa_z z^*} \tag{5}$$

in which λ, δ, and $C_{(\lambda,\delta)}$ are unknown coefficients that should be defined by applying the boundary conditions. Applying the first boundary conditions, Eq. (3), and expanding the solution into trigonometric form results in

$$\begin{aligned}\theta &= A_0 z^* \\ &+\sum_{m=1}^{\infty}\cos(\lambda\kappa_x x^*)\times[A_m\cosh(\lambda\varepsilon_H\kappa_z z^*)+B_m\sinh(\lambda\varepsilon_H\kappa_z z^*)] \\ &+\sum_{n=1}^{\infty}\cos(\delta\varepsilon\kappa_y y^*)\times[A_n\cosh(\delta\varepsilon_H\kappa_z z^*)+B_n\sinh(\delta\varepsilon_H\kappa_z z^*)] \\ &+\sum_{n=1}^{\infty}\sum_{m=1}^{\infty}\cos(\lambda\kappa_x x^*)\cos(\delta\varepsilon\kappa_y y^*) \\ &\times[A_{mn}\cosh(\beta\varepsilon_H\kappa_z z^*)+B_{mn}\sinh(\beta\varepsilon_H\kappa_z z^*)]\end{aligned} \tag{6}$$

where λ, δ, and β are eigenvalues in the form given next

$$\lambda=\frac{m\pi}{\kappa_x},\qquad \delta=\frac{n\pi}{\kappa_y\varepsilon},\qquad \beta=\sqrt{\lambda^2+\delta^2} \tag{7}$$

In Eq. (6), A and B are coefficients that should be defined by applying the boundary conditions on the top and bottom surfaces. As shown in Eq. (4), the Neumann boundary conditions on these two surfaces have a discrete form that cannot directly be applied. To apply these boundary conditions in the solution, Eq. (6), a two-dimensional (2-D) Fourier expansion technique is used. Using this technique, the temperature distribution is derived for single and multihotspots cases.

1. Single Heat Source and Heat Sink

For a plate with one heat source on the top surface (superscript t) and one heat sink on the bottom (superscript b), the coefficients of the solution, Eq. (6), are as follows

$$A_0=\frac{\kappa_z^2\varepsilon_H}{\varepsilon}s^t_{00}=\frac{\kappa_z^2\varepsilon_H}{\varepsilon}s^b_{00} \tag{8}$$

$$B_m=\frac{2\kappa_z s^t_{m0}}{\varepsilon\lambda} \tag{9}$$

$$B_n=\frac{2\kappa_z s^t_{0n}}{\varepsilon\delta} \tag{10}$$

$$B_{mn}=\frac{4\kappa_z s^t_{mn}}{\varepsilon\beta} \tag{11}$$

$$A_m=\frac{2\kappa_z}{\varepsilon\lambda}(s^b_{m0}\operatorname{csch}(\lambda\varepsilon_H)-s^t_{m0}\coth(\lambda\varepsilon_H)) \tag{12}$$

$$A_n=\frac{2\kappa_z}{\varepsilon\delta}(s^b_{0n}\operatorname{csch}(\delta\varepsilon_H)-s^t_{0n}\coth(\delta\varepsilon_H)) \tag{13}$$

$$A_{mn}=\frac{4\kappa_z}{\varepsilon\beta}(s^b_{mn}\operatorname{csch}(\beta\varepsilon_H)-s^t_{mn}\coth(\beta\varepsilon_H)) \tag{14}$$

in which the auxiliary coefficients, obtained from the Fourier expansion, are

$$s^{t/b}_{00}=\iint_{t/b}q^*_{(x,y)}\,dx^*\,dy^* \tag{15}$$

$$s^{t/b}_{m0}=\iint_{t/b}q^*_{(x,y)}\times\cos(\lambda\kappa_x x^*)\,dx^*\,dy^* \tag{16}$$

$$s^{t/b}_{0n}=\iint_{t/b}q^*_{(x,y)}\times\cos(\delta\varepsilon\kappa_y y^*)\,dy^*\,dx^* \tag{17}$$

$$s^{t/b}_{mn}=\iint_{t/b}q^*_{(x,y)}\times\cos(\lambda\kappa_x x^*)\cos(\delta\varepsilon\kappa_y y^*)\,dx^*\,dy^* \tag{18}$$

2. Multiple Sources/Sinks on Top and Bottom Surface

Because conduction heat transfer in a solid is a linear process, the superposition principle is applicable. As such, for cases with multiple sources/sinks on each of the top and bottom surfaces, temperature distribution can be readily obtained by superposing the single source results. Using this approach, the solution can be generalized for rectangular plates with M and N number of sources/sinks on the top and bottom surfaces, respectively. As a result, the solution, Eq. (6), and the coefficients, Eqs. (8–14), remain unchanged; however, the auxiliary coefficients take the more general form, in which q^* changes to q^*_i referring to multiple sources/sinks. In a particular case, in which each spot has a constant heat flux,the auxiliary coefficients take the following simplified form

$$s^{t/b}_{00}=\sum_{i=1}^{M\text{ or }N}q^*_i a^*_i b^*_i \tag{19}$$

$$s^{t/b}_{m0}=\frac{1}{\lambda\kappa_x}\sum_{i=1}^{M\text{ or }N}q^*_i b^*_i\sin(\lambda\kappa_x x^*)\Big|_{X^*_i-\frac{a^*_i}{2}}^{X^*_i+\frac{a^*_i}{2}} \tag{20}$$

$$s^{t/b}_{0n}=\frac{1}{\delta\varepsilon\kappa_y}\sum_{i=1}^{M\text{ or }N}q^*_i a^*_i\sin(\delta\varepsilon\kappa_y y^*)\Big|_{Y^*_i-\frac{b^*_i}{2}}^{Y^*_i+\frac{b^*_i}{2}} \tag{21}$$

$$s^{t/b}_{mn}=\frac{1}{\lambda\delta\varepsilon\kappa_x\kappa_y}\sum_{i=1}^{M\text{ or }N}q^*_i\sin(\lambda\kappa_x x^*)\Big|_{X^*_i-\frac{a^*_i}{2}}^{X^*_i+\frac{a^*_i}{2}}\times\sin(\delta\varepsilon\kappa_y y^*)\Big|_{Y^*_i-\frac{b^*_i}{2}}^{Y^*_i+\frac{b^*_i}{2}} \tag{22}$$

B. Thermal Resistance

To define thermal resistance, two temperatures and the amount of heat flow is required. In this study, the difference between average temperatures over the heat sources and heat sinks is considered the temperature difference required to define the thermal resistance. Total heat flow also can be derived by integrating the heat flux over the heat sources or heat sinks domain. As such, the spreading resistance can be defined as [14–16,19]

$$R^*=\frac{|\bar{\theta}_{\text{Sources}}-\bar{\theta}_{\text{Sinks}}|}{Q^*} \tag{23}$$

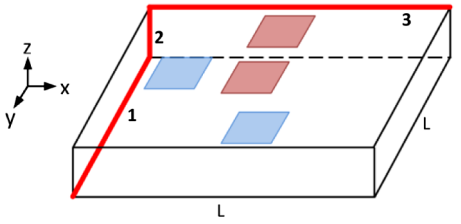

Fig. 3 Cutline position inside rectangular plate for comparison between analytical and numerical results.

where

$$\bar{\theta}_{\text{Sources}} = \frac{1}{\sum_{\text{Sources}} a_i^* b_i^*} \sum_{\text{Sources}} \int_{Y_i^*-\frac{b_i^*}{2}}^{Y_i^*+\frac{b_i^*}{2}} \int_{X_i^*-\frac{a_i^*}{2}}^{X_i^*+\frac{a_i^*}{2}} \theta_{\text{Sources}}\, \mathrm{d}x^*\, \mathrm{d}y^* \tag{24}$$

$$\bar{\theta}_{\text{Sink}} = \frac{1}{\sum_{\text{Sinks}} a_i^* b_i^*} \sum_{\text{Sinks}} \int_{Y_i^*-\frac{b_i^*}{2}}^{Y_i^*+\frac{b_i^*}{2}} \int_{X_i^*-\frac{a_i^*}{2}}^{X_i^*+\frac{a_i^*}{2}} \theta_{\text{Sink}}\, \mathrm{d}x^*\, \mathrm{d}y^* \tag{25}$$

$$Q^* = \left| \iint_{\text{Sources/Sinks}} q_i^*\, \mathrm{d}x^*\, \mathrm{d}y^* \right| \tag{26}$$

For the case of constant heat fluxes, Q^* can simply be calculated by summation of dimensionless heat fluxes multiplied by their dimensionless domain area.

III. Results and Discussion

A. Model Validation

To validate the present model, an anisotropic rectangular pyrolytic graphite sheet (PGS) with an arbitrary arrangement of four spots is assumed, i.e., two sources on the top surface and two sinks on the bottom, see Fig. 3. The chosen PGS has a through-plane and in-plane thermal conductivity of 4 and 800 W/m · K, respectively [4–6].

The numerical analysis is performed using COMSOL Multiphysics 4.2a [24]. A sensitivity study on the grid size is performed for two different levels of extra and extremely fine mesh sizes with 7.6×10^4 and 4.2×10^5 elements, respectively. Less than 0.1% relative difference for local temperature between the two cases is observed. The computation time for the extra fine mesh size using a typical Pentium dual-core PC is around 20 s. Using the proposed model, this time is less than 5 s for 100 terms in series and fine mesh size.

To compare the results quantitatively, temperatures along three different imaginary lines in three different directions, labeled in Fig. 3, are plotted in Fig. 4 for both analytical and numerical results. For this specific example, the characteristic length L and Q_0 are equal to 0.1 m and 1 kW, respectively. The reference thermal conductivity is assumed to be 4 W/m · K. The thermophysical parameters are listed in Table 1.

As shown in Fig. 4, there is an excellent agreement between the analytical model results and the numerical simulation. A sensitivity analysis on the number of eigenvalue terms in the series solution is performed. Increasing the number of terms in the series from 100 to 400 will not change the solution considerably (less than 0.1%).

B. Parametric Study

A parametric study is performed to investigate the effects of: 1) anisotropy and 2) geometrical parameters such as plate thickness, plate aspect ratio, spots relative size, and aspect ratio on thermal performance of heat spreaders. This parametric study is performed for spreaders with a single heat source and heat sink, each of them placed on one face of the plate. The behavior of the multihotspot geometries can be obtained by superposing the effects caused by each single spot.

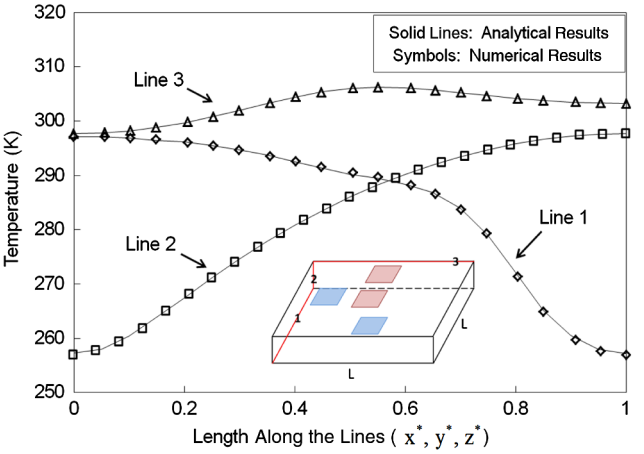

Fig. 4 Comparison between present analytical model and numerical results for temperature along three different cutlines using the hotspot arrangement of Fig. 3.

To cover a wide range of variation in each of the previously mentioned geometrical parameters and determine the effect of anisotropy, two different arrangements for source and sink are chosen to represent two extreme cases, as shown in Fig. 5. In the first case, a heat source on the top and a heat sink on the bottom are centrally aligned and positioned at the center of the plate. This arrangement (case I) represents the lowest thermal resistance due to the minimum distance between the source and the sink. In case II, the heat source on the top surface and the heat sink on the bottom surface are positioned at two opposite corners; thus representing the highest thermal resistance. Heat sources and heat sinks are assumed isoflux.

1. *Effect of Anisotropy*

To study the anisotropy of materials, resistance of a square plate with two different arrangements of source and sink, case I and case II (shown in Fig. 5) is plotted vs through-plane to in-plane conductivity ratios for four different plate thicknesses in Figs. 6 and 7. The conductivity ratio k_{xy}/k_z ranges from 0.01 to 100. The source and sink are identical squares with arbitrary side lengths of 0.2 L. The plate is also set to be square ($\varepsilon = W/L = 1$). The effect of the spots' size will be investigated separately later. For better depiction, the graphs are plotted in logarithmic scale.

Figure 6 shows that, in a plate with two centrally aligned spots on the top and bottom (case I), as the ratio of the in-plane to through-plane conductivity increases, the thermal resistance decreases. This trend can be explained as follows: as the in-plane conductivity increases, the temperature becomes uniform over the surface much faster due to less in-plane resistance against the heat flow, so the heat spreading/constriction takes place easier with less temperature drop.

For the arrangement of case I, heat transfer improvement due to increasing the in-plane conductivity is directly related to the size of the spots. As shown in Fig. 8, for smaller spot area, the resistance

Table 1 Thermophysical characteristics of plate and spots in Fig. 3 used in numerical analysis

Plate dimensions	Plate material	Source 1	Source 2	Sink 1	Sink 2
$L = 10$ cm	$k_0 = 4$ W/mk		$Q_0 = 1$ kW		
$\varepsilon = 1$	$\kappa_x = 0.07$	$a^* = 0.2$	$a^* = 0.2$	$a^* = 0.2$	$a^* = 0.2$
$\varepsilon_H = 0.2$	$\kappa_y = 0.07$	$b^* = 0.2$	$b^* = 0.2$	$b^* = 0.2$	$b^* = 0.2$
	$\kappa_z = 1$	$X^* = 0.5$	$X^* = 0.5$	$X^* = 0.5$	$X^* = 0.2$
		$Y^* = 0.5$	$Y^* = 0.8$	$Y^* = 0.5$	$Y^* = 0.9$
		$q^* = 1$	$q^* = 1$	$q^* = 1$	$q^* = 1$

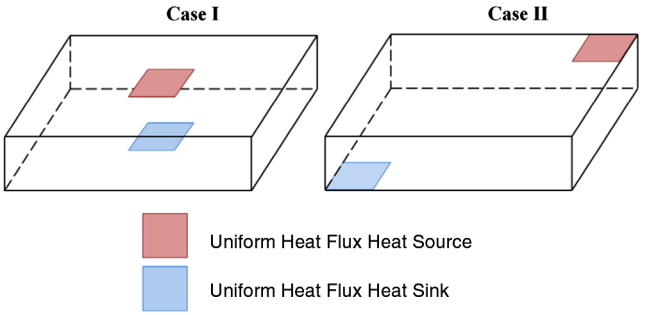

Fig. 5 Two different arrangements of hotspots for parametric study.

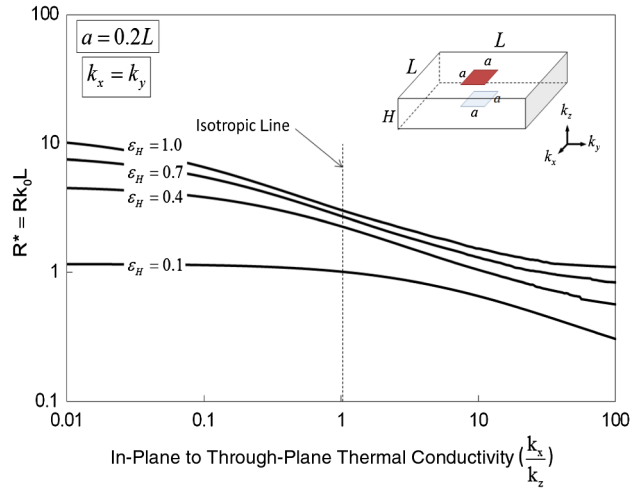

Fig. 6 Resistance vs in-plane to through-plane conductivity ratio for four thicknesses (case I).

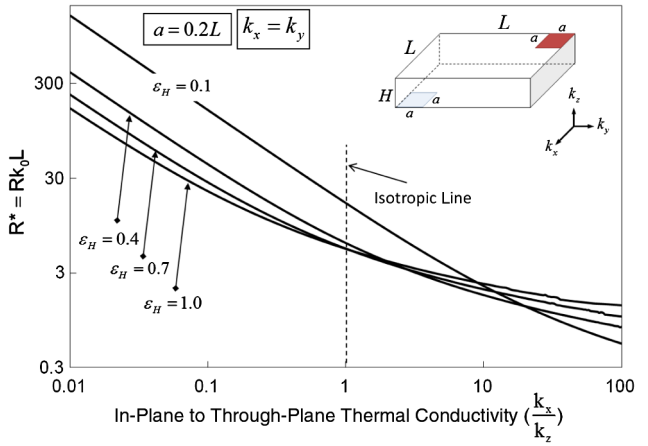

Fig. 7 Resistance vs in-plane to through-plane conductivity ratio for four thicknesses (case II).

decrease occurs more significantly when the in-plane thermal conductivity increases. This is because the spreading/constriction resistance becomes more considerable with smaller relative spot sizes. Thus, in such spreaders, higher in-plane thermal conductivity results in much better thermal performance improvement of the heat spreader. In other words, for smaller spots, it is thermally more efficient to use anisotropic material for the spreader. At the limit where the spots' sizes are as big as the plate surface, i.e., one-dimensional (1-D) heat conduction, no spreading or constriction exists; thus, changing the in-plane conductivity has no effect on the plate resistance.

For the second arrangement (case II), anisotropy of the material has a more pronounced effect on the thermal performance of the spreader. Figure 7 shows, for all thicknesses, thermal resistance decreases as the in-plane conductivity increases. For thinner plates, this variation

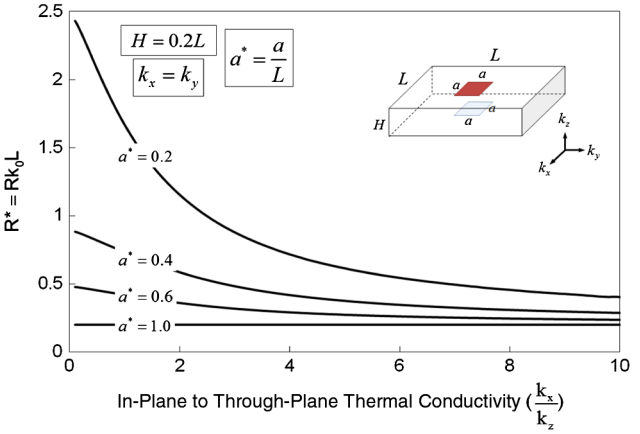

Fig. 8 Resistance vs in-plane to through-plane conductivity ratio for four hotspot sizes (case I).

is more than for the thicker ones. It is because in thinner plates the heat is passing through a smaller cross section which in comparison to thicker plates results in higher thermal resistance. However, as the in-plane thermal conductivity increases, the effect of in-plane resistance becomes less important and the thickness becomes the controlling parameter. This phenomenon is clearly shown in Fig. 7, where two curves of different thicknesses intersect. These intersection points demarcate the critical conductivity ratios for the two corresponding thicknesses before which the in-plane resistance is dominant, thus the thinner plate has a larger resistance. However, beyond these points, through-plane heat transfer plays a more important role, and the thicker plate presents more resistance.

The important points can be summarized as follows:

1) Regardless of spot arrangement and plate thickness, increasing the in-plane thermal conductivity always improves the heat transfer.

2) As the relative eccentricity of spots on the top and bottom surface increases, the anisotropy effect becomes more prominent.

3) As the relative size of spots becomes smaller, increasing the in-plane thermal conductivity has a more pronounced effect on the thermal performance of the plate.

4) Changing anisotropy in thinner plates creates more resistance variation compared to thicker ones.

5) In 1-D heat transfer, resistance is only a function of through-plane conductivity and the plate material's anisotropy has no effect on its resistance.

2. *Geometrical Parametric Study*

In this section, for convenience, all cases are assumed isotropic.

a. Effect of Plate Thickness.—Dimensionless resistance vs dimensionless thickness for five arbitrary different sizes of spots is plotted for both cases I and II in Figs. 9 and 10, respectively. Heat source and heat sink in each case are assumed to be square and have the same size. The plate is also set to be square.

As indicated in Figs. 9 and 10, two asymptotes can be recognized. It is shown that in case I, in which the source and sink are vertically aligned, as the thickness of the plate approaches zero, the resistance with an increasing slope moves to zero. The slope at very small thickness approaches the inverse of the spot area for each spot size. It can be interpreted that for case I, at smaller thickness, the heat transfer approaches a 1-D conduction, in which the resistance is proportional to the thickness and the inverse of the area. In other words, if the plate is thin enough, heat only passes through the column between the source and sink, i.e., a 1-D heat conduction. However, this is not true for case II, in which the source and sink are positioned at the corners. In this case, as the thickness approaches zero, the resistance approaches infinity due to the very narrow heat transfer path, as shown in Fig. 10.

On the other extreme, when the plate thickness increases to large values, similar behavior is observed for both cases I and II. It is seen

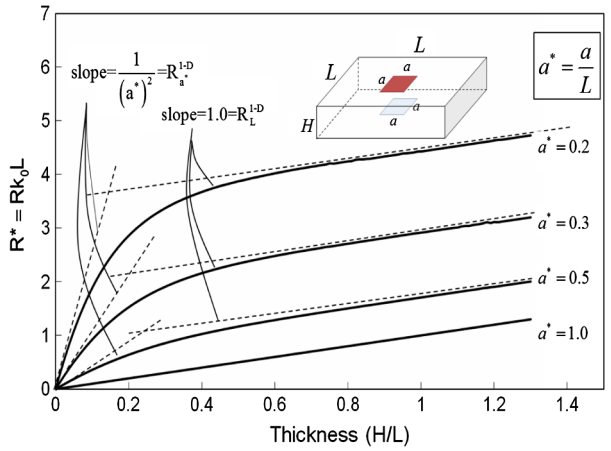

Fig. 9 Plate resistance vs plate thickness for hotspot arrangement of case I.

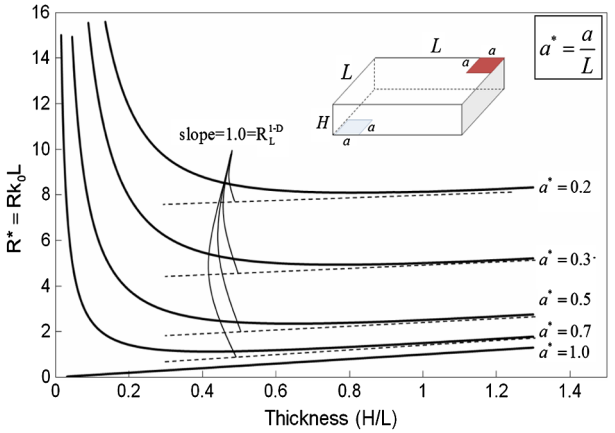

Fig. 10 Plate resistance vs plate thickness for hotspot arrangement of case II.

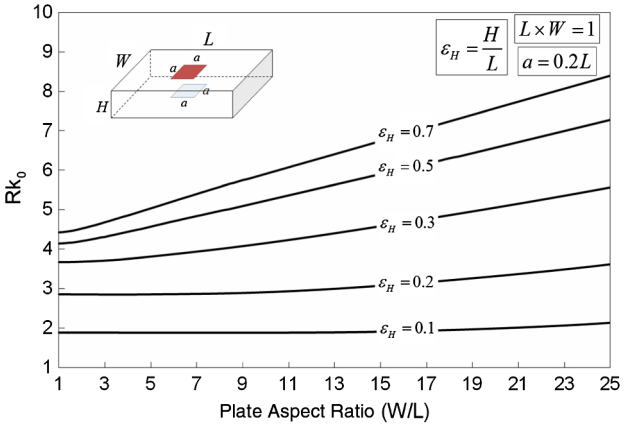

Fig. 11 Plate resistance vs plate aspect ratio for different thickness (case I).

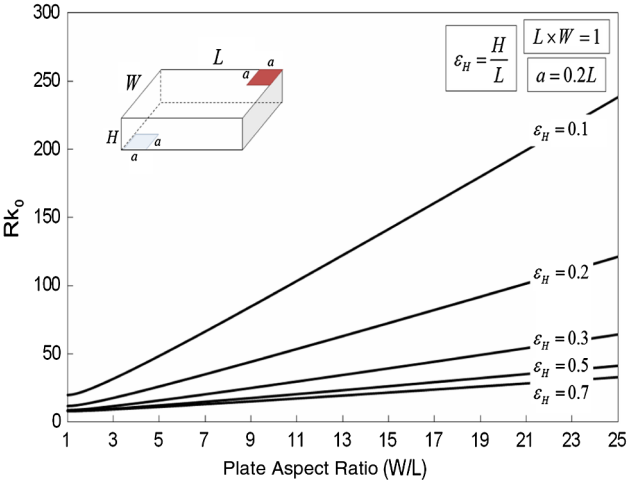

Fig. 12 Plate resistance vs plate aspect ratio for different thickness (case II).

that for thick plates, resistance varies almost linearly with thickness and the rate of change approaches unity, which means any increase in the thickness is equivalent to adding the resistance of a 1-D heat transfer in a block with the dimensions of plate area and that increased thickness. This can be explained as follows: as the thickness increases beyond a value, the resistance increase is not a function of spot size and position anymore and it changes only with thickness.

Also, note that for the spreaders with eccentric spots, there always is an optimum thickness that provides a minimum resistance and is a function of plate geometry and spot arrangement. The following summarizes the effects of plate thickness:

1) For large thicknesses, the resistance variation due to the thickness change is not a function of spot arrangements.

2) Resistance for plates with nonaligned spots on the top and bottom surfaces approaches infinity as the thickness approaches zero.

3) Resistance for the plate with aligned and equal spots on the top and bottom surfaces becomes independent of plate size and spot position as the thickness approaches zero.

4) For plates with nonaligned spots on the top and bottom surfaces, there is an optimum thickness, which gives a minimum resistance. As the size of the spots decreases, this optimum value increases.

5) Resistance for plates with aligned and equal spots on the top and bottom surfaces has an asymptotic behavior in both very small and very large thicknesses.

b. Effect of Plate Aspect Ratio.—The effect of the plate aspect ratio on the resistance for both cases I and II for different thicknesses are shown in Figs. 11 and 12, respectively. The area of the plate $W \times L$ is kept constant, equal to unity. The source and sink dimensions remain constant and equal in both cases, $a = b = a' = b' = 0.2L$.

In this specific case, because the goal is to investigate the effect of variation of L, which has been used as the characteristic length, nondimensionalizing the resistance with respect to L would not lead to any useful results. Therefore, dimensional resistances are plotted.

Figure 11 shows the resistance of constant area plate vs its aspect ratio with identical spots in the center. It can be seen that regardless of the thickness, increasing the aspect ratio deteriorates the thermal performance. However, as the thickness of the plate decreases, the effect of the aspect ratio variation becomes smaller. The reason is that heat transfer occurs mainly through the plate bulk, which is in between the sink and the source. Thus, changing the aspect ratio does not noticeably affect the heat transfer.

Similar to case I, but more strongly, increasing the aspect ratio for the spot arrangement of case II increases the resistance, as shown in Fig. 12. This is reasonable because as the aspect ratio increases, two spots get further away from each other so the heat flow coming from the source has to pass through a longer distance to reach the sink. The following are the important conclusions regarding the plate aspect ratio:

1) For a fixed area of heat spreader, a square shape offers minimum resistance.

2) Changing the plate aspect ratio causes smaller resistance change in thicker plates rather than thinner ones.

c. Effect of Source/Sink Relative Size.—In applications where the spot sizes are adjustable, they can be chosen such that thermal resistance is minimized. For this purpose, the effect of the spot relative size on the plate resistance is studied on case I for two different scenarios: 1) the square-shaped source and sink vary in size simultaneously and

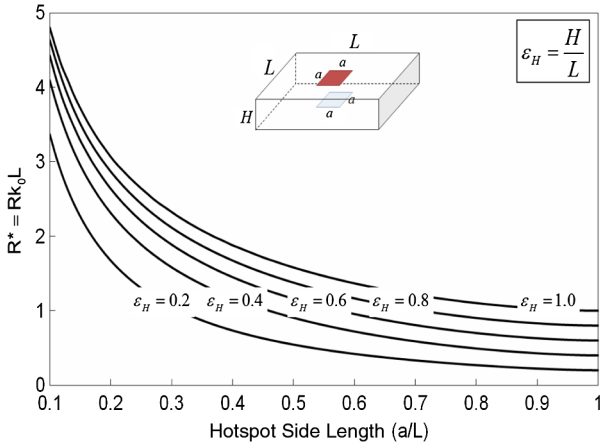

Fig. 13 Plate resistance vs hotspot size for case I (source and sink vary in size equally).

2) the sink size is kept constant at $a' = b' = 0.2L$, whereas the source size is varied.

For the first scenario, the resistance vs side length of square source and sink is plotted in Fig. 13 for different thicknesses. As can be seen, the spot side length ranges from small values to unity, i.e., the plate length.

Figure 13 shows that as the heat sink and heat source size increase, the resistance against the heat flow decreases. At the point where the dimensionless spot side length is equal to unity the area of spots are equal to the area of the plate, the heat transfer is 1-D and the dimensionless resistance is equal to the dimensionless thickness.

The second scenario is plotted in Fig. 14. When one of the spots has a constant area, increasing the other spot's size does not always cause heat transfer improvement. It shows that the minimum resistance occurs when the sink area is between the heat source and the spreader plate area. This optimum point depends on the geometrical parameters of the plates and the source. One important parameter in defining this optimum point is the thickness of the plate. As indicated in Fig. 14, the minimum resistance happens at larger heat source areas as the thickness increases. There is a critical thickness, beyond which this optimum resistance occurs, where the source has the biggest possible area, i.e., the plate surface area. For instance, when the square heat source has a constant side length of $0.2L$, this critical thickness is almost $0.3L$. Beyond this value, the minimum resistance occurs when the sink area is equal to plate area.

The important points regarding the spots size (case I) can be concluded as follows:

1) For the same heat source and heat sink size, a minimum thermal resistance exists where there is maximum available area.

2) If one of the spots areas is fixed, there is an optimum size for the other spot that offers a minimum resistance. This optimum size is somewhere between the fixed spot size and the spreader plate size.

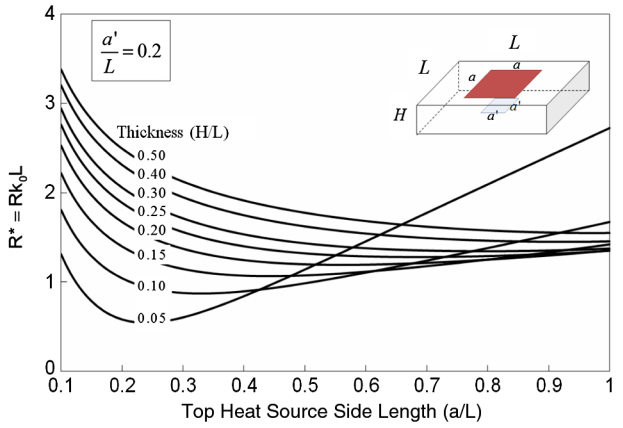

Fig. 14 Plate resistance vs heat sink size for case I.

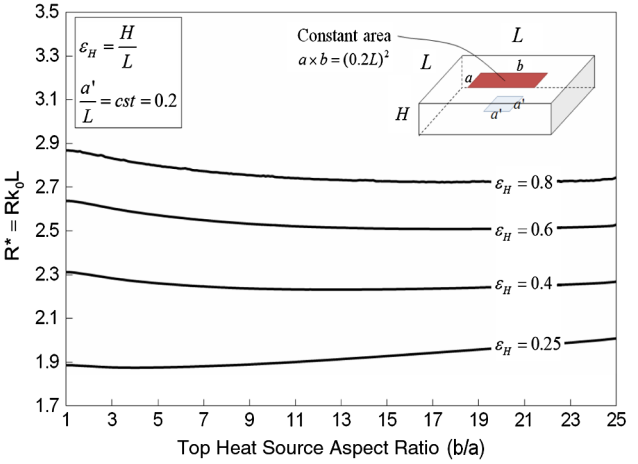

Fig. 15 Plate resistance vs heat sink aspect ratio for case I (source size remains constant).

3) Beyond some thicknesses, the minimum resistance occurs when the spots have the maximum available area.

d. Effect of Source/Sink Aspect Ratio.—The spot aspect ratio also can affect the resistance of the plate. Resistance vs heat sink aspect ratio, while its area is kept constant, is plotted in Fig. 15 for case I for different plate thickness. All other geometrical parameters, including the sink's dimensions, are kept constant. The aspect ratio changes from 1, a square of $0.2L \times 0.2L$, to 25, which is a strip with the length of the plate width. The plot in Fig. 15 shows that if one hotspot is confined to a square shape, the minimum resistance occurs when the other spot has a rectangular shape and its aspect ratio depends on the plate thickness and square spot's size and area. As can be seen in Fig. 15, as the thickness of the plate increases, the optimum aspect ratio of the source increases.

The following summarizes the trends observed in Fig. 15:

1) If one spot is confined to a constant square shape, the minimum resistance occurs when the other spot has a rectangular shape and its aspect ratio depends on the plate thickness and square spot size and area.

2) As the plate thickness increases, the optimum aspect ratio for the heat sink while the heat source is in square shape increases.

3) Comparing to other parameters spot's aspect ratio has less impact on thermal resistance.

IV. Conclusions

A new analytical model was developed for temperature distribution inside anisotropic rectangular plates subjected to multiple sources and sinks on the top and bottom surfaces. A 2-D Fourier expansion technique was used to transform the discrete Neumann boundary conditions on the top and bottom into a continuous form. The solution was first developed for the case with an arbitrary single spot on each side and then, using the superposition principle, it was extended to the general form to cover multispot cases. The model was validated by an independent numerical simulation data and a perfect agreement was observed. Thermal spreading resistance was then defined for the plate and a comprehensive parametric study for optimization purpose was performed. The effects of both thermal and geometrical parameters on the resistance were discussed in detail.

Acknowledgments

The author gratefully acknowledges the financial support of the Natural Science and Engineering Research Council of Canada (grant no. 31-614094) and Alpha Technologies-Sponsored Research (grant no. 31-569228).

References

[1] Kuo, W., Wu, T., Lu, H., and Lo, T., "Microstructures and Mechanical Properties of Nano-Flake Graphite Composites," *16th International Conference on Composite Materials*, Kyoto, Japan, 2007.

[2] Dai, L., "Functionalization of Graphene for Efficient Energy Conversion and Storage," *Accounts of Chemical Research*, Vol. 46, No. 1, 2013, pp. 31–42. doi:10.1021/ar300122m

[3] Chung, D. D. L., and Takizawa, Y., "Performance of Isotropic and Anisotropic Heat Spreaders," *Journal of Electronic Materials*, Vol. 41, No. 9, Sept. 2012, pp. 2580–2587. doi:10.1007/s11664-012-2177-4

[4] Norley, J., Tzeng, J., and Getz, G., "The Development of a Natural Graphite Heat-Spreader," *Seventeenth Annual IEEE Symposium on Semiconductor Thermal Measurement and Management*, IEEE, Piscataway, NJ, March 2001, pp. 107–110. doi:10.1109/STHERM.2001.915157

[5] Taira, Y., Kohara, S., and Sueoka, K., "Performance Improvement of Stacked Graphite Sheets for Cooling Applications," *58th Electronic Components and Technology Conference*, IEEE, Piscataway, NJ, May 2008, pp. 760–764. doi:10.1109/ECTC.2008.4550059

[6] Panasonic Electronic Devices Co., "Pyrolitic Graphite Sheet," http://www.panasonic.com/industrial/demo/en_demo.asp [retrieved 25 March 2014].

[7] Kelly, K. F., and Billups, W. E., "Synthesis of Soluble Graphite and Graphene," *Accounts of Chemical Research*, Vol. 46, No. 1, Jan. 2013, pp. 4–13. doi:10.1021/ar300121q

[8] Yovanovich, M. M., Muzychka, Y. S., and Culham, J. R., "Spreading Resistance of Isoflux Rectangles and Strips on Compound Flux Channel," *Journal of Thermophysics and Heat Transfer*, Vol. 13, No. 4, 1999, pp. 495–500. doi:10.2514/2.6467

[9] Karmalkar, S., Mohan, P. V., and Kumar, B. P., "A Unified Compact Model of Electrical and Thermal 3-D Spreading Resistance Between Eccentric Rectangular and Circular Contacts," *Electron Device Letters*, Vol. 26, No. 12, Dec. 2005, pp. 909–912. doi:10.1109/LED.2005.859627

[10] Kokkas, A. G., "Thermal Analysis of Multiple-Layer Structures," *IEEE Transactions on Electron Devices*, Vol. ED-21, No. 11, 1974, pp. 674–681. doi:10.1109/T-ED.1974.17993

[11] Kadambi, V., and Abuaf, N., "An Analysis of the Thermal Response of Power Chip Packages," *IEEE Transactions on Electron Devices*, Vol. ED-32, No. 6, 1985, pp. 1024–1033. doi:10.1109/T-ED.1985.22068

[12] Albers, J., "An Exact Recursion Relation Solution for the Steady-State Surface Temperature of a General Multilayer Structure," *IEEE Transactions on Components, Packaging, and Manufacturing Technology: Part A*, Vol. 18, No. 1, March 1995, pp. 31–38. doi:10.1109/95.370732

[13] Culham, J. R., Yovanovich, M. M., and Lemczyk, T. F., "Thermal Characterization of Electronic Packages Using a Three-Dimensional Fourier Series Solution," *Journal of Electronic Packaging*, Vol. 122, No. 3, 2000, pp. 233–239. doi:10.1115/1.1287928

[14] Muzychka, Y. S., Culham, J. R., and Yovanovich, M. M., "Thermal Spreading Resistances in Rectangular Flux Channels Part II. Edge Cooling," *36th AIAA Thermophysics Conference*, Orlando, FL, 2003, pp. 1–9.

[15] Muzychka, Y. S., Culham, J. R., and Yovanovich, M. M., "Thermal Spreading Resistance of Eccentric Heat Sources on Rectangular Flux Channels," *Journal of Electronic Packaging*, Vol. 125, No. 2, 2003, pp. 178–185. doi:10.1115/1.1568125

[16] Muzychka, Y. S., "Influence Coefficient Method for Calculating Discrete Heat Source Temperature on Finite Convectively Cooled Substrates," *IEEE Transactions on Components and Packaging Technologies*, Vol. 29, No. 3, Sept. 2006, pp. 636–643. doi:10.1109/TCAPT.2006.880477

[17] Rahmani, Y., and Shokouhmand, H., "A Numerical Study of Thermal Spreading/Constriction Resistance of Silicon," *13th IEEE Intersociety Conference on Thermal and Thermomechanical Phenomena in Electronic Systems (ITherm)*, IEEE, Piscataway, NJ, 2012, pp. 482–486. doi:10.1109/ITHERM.2012.6231470

[18] Rahmani, Y., and Shokouhmand, H., "Assessment of Temperature-Dependent Conductivity Effects on the Thermal Spreading/Constriction Resistance of Semiconductors," *Journal of Thermophysics and Heat Transfer*, Vol. 26, No. 4, 2012, pp. 638–643. doi:10.2514/1.T3828

[19] Dan, B., Geer, J. F., and Sammakia, B. G., "Heat Conduction in a Rectangular Tube with Eccentric Hot Spots," *Journal of Thermal Science and Engineering Applications*, Vol. 3, No. 4, 2011, Paper 041002. doi:10.1115/1.4005143

[20] Ying, T. M., and Toh, K. C., "A Heat Spreading Resistance Model for Anisotropic Thermal Conductivity Materials in Electronic Packaging," *The Seventh Intersociety Conference on Thermal and Thermomechanical Phenomena in Electronic Systems*, Vol. 1, IEEE, Piscataway, NJ, 2000, pp. 314–321. doi:10.1109/ITHERM.2000.866842

[21] Muzychka, Y. S., Yovanovich, M. M., and Culham, J. R., "Thermal Spreading Resistance in Compound and Orthotropic Systems," *Journal of Thermophysics and Heat Transfer*, Vol. 18, No. 1, Jan. 2004, pp. 45–51. doi:10.2514/1.1267

[22] Muzychka, Y. S., "Spreading Resistance in Compound Orthotropic Flux Tubes and Channels with Interfacial Resistance," *Journal of Thermophysics and Heat Transfer*, Vol. 28, No. 2, April 2014, pp. 313–319. doi:10.2514/1.T4203

[23] Muzychka, Y. S., "Thermal Spreading Resistance in Compound Orthotropic Circular Disks and Rectangular Channels with Interfacial Resistance," *44th AIAA Thermophysics Conference*, San Diego, CA, 2013, pp. 1–11.

[24] "COMSOL Multiphysics 4.2a," COMSOL, Stockholm, Sweden, http://www.comsol.com/4.2a/ [retrieved 25 March 2014].